RESEARCH ARTICLE

Analysis of Extinction in a Non-Premixed Turbulent Flame using Large Eddy Simulation and the Chemical Explosion Mode Analysis

I. A. Dodoulas and S. Navarro-Martinez

(*Received 00 Month 200x; final version received 00 Month 200x*)

The paper presents computational results of a turbulent non-premixed flame with large extinction, using the LES-PDF methodology. The simulation captures local flame extinction at different flame locations and major species predictions shows good agreement with experimental data. A Chemical Explosive Mode Analysis is used to determine the flame structure including the explosive modes and the Damköhler number distribution. Due to the nature of the turbulence combustion model, statistical information of the sub-grid flame structure is available: such as sub-grid explosive modes. The analysis suggests that in the present flame, sub-grid structures are only relevant close to the inlet nozzle and downstream extinction is governed by large scale interactions.

1. Introduction

Flame extinction is characterised by complex interactions between chemical reactions and the turbulent flow. Turbulence introduces fluctuations (temporal and spatial) in thermodynamic quantities, such as the temperature and species concentrations, and therefore fluctuations in the respective reaction rates. The fluctuations affect the exothermic reactions that sustain combustion and the flame can locally "quench" and form extinction spots or pockets. In these spots, the mixture-density locally increases and molecular viscosity drops, therefore increasing the Reynolds number and destabilising the flow-field. High Reynolds number flames always have extinction pockets and as the inlet velocity approaches the blow-off velocity the pockets become larger before the flame fully extinguishes.

This "feedback" between flow and chemistry, together with the fact that extinction is a finite-rate chemistry effect, makes modelling flame with extinction very difficult. An example of this complexity is the Sandia series of methane non-premixed flames [34]. The moderate Reynolds number Sandia D flame has been successfully predicted by a large number of researchers. However, the higher Reynolds flame Sandia F, where large extinction is present, has been much less successful and only a handful of calculations exist [5, 11, 15]. Methods based on the solution of the scalar Probability Density Function (PDF) [9, 30] are very general and had some success in modelling flame extinction. In the RANS context, flames with extinction are sensitive to the micro-mixing model as well as the associated time-scale [5, 24]. This is due to the fact that the micro-mixing model has to reproduce all the extinction that occurs at all scales. In Large Eddy Simulation (LES) context, modelling uncertainties are alleviated due to the fact that time fluctuations are well resolved and sub-grid fluctuations are small.

Although some turbulent-combustion models are able to capture extinction, there is a limited information on why models fail or succeed to do it. Extinction can be clearly identified experimentally. However, in computer simulations, it cannot be

2

easily separated from the turbulence model: It can be only seen directly on the filtered (super-grid) scales. In some points, the filtered quantities may suggest a burning solution, however extinction 'spots' can exist at levels below the grid scales. This *sub-grid* extinction depends on the turbulence-combustion model used and it cannot be identified by looking only at filtered quantities and a sub-grid measure is needed.

The objective of the present work is to apply the LES-PDF [10] methodology to study extinction in a non-premixed flame and use *a-posteriori* Flame Diagnostics to identify the flame structure and extinction characteristics. To solve the PDF equation, the Stochastic Field Monte Carlo method [38] is used. Mustata *et al.* [26] implemented the Stochastic Fields in LES and the method was successfully applied in a wide range of combustion problems: Non-premixed [13, 15] and premixed flames [8, 16], flame extinction [15] and flame autoignition [31]. The Flame Diagnostics is based on the Chemical Explosive Mode Analysis (CEMA) [18, 20]. CEMA is based on the eigenvalue decomposition analysis of the chemistry source term; where most reactive modes are identified. The analysis is local and, unlike Flame Index [25], does not depend on scalar gradients. Due to the nature of the stochastic field, sub-grid flame characteristics can be extracted directly from CEMA and the presence or not of sub-grid extinction determined.

2.   Modelling

2.1   LES Modelling

Using a conventional filtering operation with filter width Δ, the filtered Navier-Stokes equations (mass and momentum) are given by:

$$\frac{\partial \overline{\rho}}{\partial t} + \frac{\partial \overline{\rho}\widetilde{u}_i}{\partial x_i} = 0 \tag{1}$$

$$\frac{\partial \overline{\rho}\widetilde{u}_i}{\partial t} + \frac{\partial \overline{\rho}\widetilde{u}_i\widetilde{u}_j}{\partial x_j} = -\frac{\partial \overline{p}}{\partial x_i} + \frac{\partial \widetilde{\tau}_{ij}}{\partial x_j} - \frac{\partial \widetilde{\tau}_{ij}^{sgs}}{\partial x_j} \tag{2}$$

Equation (2) needs closures for the sub-grid contribution. In this work the standard Smagorinsky model [36] is used, where the sub-grid stresses are assumed proportional to the filtered strain rate $\widetilde{S}_{ij}$. The proportionality constant has the dimensions of viscosity and is referred to as turbulent (or sub-grid) viscosity μ_{sgs}. The sub-grid viscosity is given by the following equation:

$$\mu_{sgs} = \overline{\rho}(C_s\Delta)^2||S_{ij}|| \tag{3}$$

where C_s is the Smagorinsky constant, taken as $C_s = 0.09$ in the present work [7], and $||S_{ij}|| = \sqrt{2\widetilde{S}_{ij}\widetilde{S}_{ij}}$ is the Frobenius norm of the resolved strain tensor.

2.2   Filtered Probability Density Function

At low Mach numbers, neglecting pressure variations and assuming unity Lewis number; the species mass fraction and enthalpy equations can be expressed as

$N_s + 1$ (number of species considered plus enthalpy) convection–diffusion–reaction equations of a generic reactive scalar ϕ. The *unfiltered* equation for ϕ is:

$$\frac{\partial \rho \phi_k}{\partial t} + \frac{\partial \rho \phi_k u_j}{\partial x_j} = \frac{\partial}{\partial x_j}\left[\rho D \frac{\partial \phi_k}{\partial x_j}\right] + \rho \dot{\omega}_k(\underline{\phi}) \tag{4}$$

where D is the molecular diffusion coefficient and $\dot{\omega}_k$ is the chemical source term of scalar k (or volumetric heat source terms in the enthalpy equation).

Using the same filtering operation, a density weighted sub-grid (or filtered) PDF for the N_{s+1} scalar quantities needed can be defined as follows:

$$\bar{\rho}\widetilde{P}\left(\mathbf{x}, t; \underline{\psi}\right) = \int_V \rho \prod_{k=1}^{N_s+1} \delta\left(\psi_k - \phi_k(\mathbf{x}, t)\right) G(\mathbf{x} - \mathbf{x'}; \Delta)\mathrm{d}\mathbf{x'} \tag{5}$$

where ψ_k represents the sample space of the k-th scalar. The modelled transport equation for the filtered PDF is (see Jones and Navarro-Martinez [14]):

$$\bar{\rho}\frac{\partial \widetilde{P}}{\partial t} + \bar{\rho}\widetilde{u}_j \frac{\partial \widetilde{P}}{\partial x_j} - \frac{\partial}{\partial x_j}\left[\bar{\rho}D_e \frac{\partial \widetilde{P}}{\partial x_j}\right]$$
$$= -\sum_{k=1}^{N_s+1} \frac{\partial}{\partial \psi_k}\left[\bar{\rho}\dot{\omega}_k(\underline{\psi})\widetilde{P}\right] - \frac{\bar{\rho}}{T_{sgs}}\sum_{k=1}^{N_s+1}\frac{\partial}{\partial \psi_k}\left[\left(\psi_k - \widetilde{\phi}_k\right)\widetilde{P}\right] \tag{6}$$

where the spatial, temporal and scalar dependencies have been dropped for compactness. A gradient approach has been applied to model the PDF transport by sub-grid turbulent fluctuations. The combined molecular diffusion and turbulent transport coefficient is given by an *effective* diffusion coefficient, $\bar{\rho}D_e = \bar{\rho}D + \mu_{sgs}/Sc_{sgs}$ [14], where Sc_{sgs} is a sub-grid Schmidt number assigned the value 0.7 [3]. The Linear Mean Square Estimation (LMSE) closure has been used [9], where the sub-grid mixing time scale T_{sgs} is assumed proportional to the velocity time scale (with $C_\phi = 2$)

$$\frac{1}{T_{sgs}} = C_\phi \frac{\mu + \mu_{sgs}}{\bar{\rho}\Delta^2} \tag{7}$$

2.3   Stochastic Field Method

The density weighted sub-grid PDF is represented by an ensemble of N stochastic fields $\xi_k^n(\mathbf{x}, t)$ such that:

$$\widetilde{P}\left(\mathbf{x}, t; \underline{\psi}\right) = \frac{1}{N}\sum_{k=1}^{N}\prod_{k=1}^{N_s+1} \delta[\psi_k - \xi_k^n(\mathbf{x}, t)] \tag{8}$$

A system of stochastic partial differential equations (SPDE) for the stochastic fields can be derived. The derived system is equivalent to the PDF equation (6). Following an Ito interpretation, the corresponding SPDEs are (see Valiño [38]):

4

$$d\xi_k^n + \widetilde{u}_j \frac{\partial \xi_k^n}{\partial x_j} dt - \frac{1}{\bar{\rho}} \frac{\partial}{\partial x_j} \left[\bar{\rho} D_e \frac{\partial \xi_k^n}{\partial x_j} \right] dt =$$

$$\dot{\omega}_k \left(\underline{\xi} \right) dt - \frac{dt}{T_{sgs}} \left(\xi_k^n - \widetilde{\phi}_k \right) + \sqrt{2 D_e} \frac{\partial \xi_k^n}{\partial x_j} dW_j^n \quad (9)$$

The last term of this equation includes dW_j^k, which represents increments of a Wiener process with 0 mean and variance dt. The stochastic term is different for each stochastic field and independent of the spatial location. The solutions of (9) preserve the bounds of the scalar as the gradient of the stochastic fields tend to zero as the scalar approach extrema values [32]. Each field therefore satisfies the mass conservation of the modelled scalar equation (4) and therefore the stochastic field species mass fractions will remain positive and sum to unity. The Favre filtered values of a k-scalar are simply obtained by ensemble averaging the corresponding stochastic fields:

$$\widetilde{\phi}_k = \frac{1}{N} \sum_{n=1}^{N} \xi_k^n \quad (10)$$

Higher moments, such as sub-grid variance, can also be easily obtained viz

$$\widetilde{\phi_{sgs,k}^2} = \frac{1}{N} \sum_{n=1}^{N} (\xi_k^n)^2 - (\widetilde{\phi}_k)^2 \quad (11)$$

2.4   Numerical Implementation

In the present work, the LES equations are solved for the flow and reactive scalar fields using the in-house code BOFFIN [17] in cylindrical coordinates. It is based on a fully implicit low Mach number formulation using a staggered arrangement. Central differences have been used in the momentum equations. The flow solver is then marched in time using a Crank-Nicholson scheme. For the reactive scalars, the spatial gradient of the stochastic term is discretized using central differences and the advection term is solved using a TVD scheme to avoid non-physical overshoots. The Wiener process (or random walk) is approximated by time step increments $dW_j^n = \sqrt{dt} \cdot r_j^n$, where $r_j^n = \{-1, 1\}$ is a dichotomic random vector.

2.5   Chemical Explosion Mode Analysis

Computational Flame Diagnostics (CFLD) are systematic tools to extract information from simulated flames. The Chemical Explosive Mode Analysis (CEMA) is a recent CFLD [20] that has been applied to flames with multi-step chemistry mechanisms. The first CEMA was applied to DNS of turbulent lifted hydrogen jet flame in a heated co-flow [20], promptly followed by similar studies on non-premixed ignition, laminar flame propagation, ignition/extinctions in perfectly stirred reactors and stabilisation mechanism studies of a turbulent lifted ethylene jet [18, 35, 39, 40]. CEMA is an eigenvalue analysis of the chemical source term Jacobian. CEMA is relatively simple to implement as it only depends on the local thermodynamic states.

It was found to be advantageous to detect critical flame phenomena compared with methods based on temperature or species concentrations [35].

For a general chemically reacting system, the conservation equations (4) can be rewritten in the following form:

$$\frac{D\phi_k}{Dt} \equiv \mathcal{L}_k = \dot{\omega}_k(\underline{\phi}) + \mathcal{S}_k(\underline{\phi}) \tag{12}$$

where $\mathcal{S}$ is the generic mixing source term; including molecular and turbulent diffusion and micro-mixing (if present). The Jacobian of the RHS of (12) has two contributions, arising from the chemical source term and the mixing term respectively,:

$$J^{ij} = \frac{\partial \mathcal{L}_k}{\partial \phi_j} \equiv \mathbf{J}_\omega + \mathbf{J}_s \tag{13}$$

where the chemical and mixing Jacobians are

$$J_\omega^{ij} = \frac{\partial \dot{\omega}_i}{\partial \phi_j} \quad J_S^{ij} = \frac{\partial \mathcal{S}_i}{\partial \phi_j} \tag{14}$$

The full Jacobian, $\mathbf{J}$, (size $N_s + 1 \times N_s + 1$) contains all the information of the system and can be used to study the dynamics of the system, for example flame stability. In a similar way, the chemical Jacobian $\mathbf{J}_\omega$ contains all the chemistry-related information and can be used to detect flame features associated with drastic spatial and/or temporal changes. CEMA uses only the chemical Jacobian and, unlike the mixing source term $\mathcal{S}$, it involves only local information of the thermodynamic variables, $\underline{\phi}$.

CEMA computes the eigenvalues of $\mathbf{J}_\omega$ for a particular state $\underline{\phi}$. The real parts of the eigenvalues, λ_k, are assumed to be sorted in descending order without loss of generality. λ_e is the first eigenvalue and is defined as a Chemical Explosive Mode (CEM) if it has a positive real part, $Re(\lambda_e) > 0$. The explosive mode can be expressed as a function of the associated eigenvectors:

$$\lambda_e = \mathbf{b_e} \mathbf{J}_\omega \mathbf{a_e} \tag{15}$$

where $\mathbf{b_e}$ and $\mathbf{a_e}$ are the left and right eigenvectors respectively.

For detailed chemical mechanisms, two extra quantifications of the CEM can be defined: The vector of Explosion Indices, $\mathbf{EI}$, and the vector of Participation Indices, $\mathbf{PI}$, defined by

$$\mathbf{EI} = \frac{\left| \mathbf{a_e} \times \mathbf{b_e^T} \right|}{sum \left(\left| \mathbf{a_e} \times \mathbf{b_e^T} \right| \right)} \tag{16}$$

$$\mathbf{PI} = \frac{\left| (\mathbf{b_e} \cdot \mathbf{SC}) \times \mathbf{R} \right|}{sum \left((\mathbf{b_e} \cdot \mathbf{SC}) \times \mathbf{R} \right)} \tag{17}$$

where **SC** is the stoichiometric coefficient matrix and **R** is the vector of the net rates for the reactions and $\times$ denotes element-wise multiplication of two vectors. **EI** indicates the normalized contribution of each species to the CEM and **PI** the normalized contribution of each reaction to the CEM. The definitions of **EI** and **PI** are similar to the radical pointer and participation index, respectively, in the Computational Singular Perturbation (CSP) theory [12].

The existence of a CEM indicates the propensity of the mixture to auto-ignite if it is put in an isolated environment [35]. The transition of a mode from explosive, i.e. $Re(\lambda_e) > 0$ to non-explosive, i.e. $Re(\lambda_e) < 0$ is strongly correlated to critical flame features such as ignition, extinction and premixed flame front locations [21]. The above observation can be used for CFLD of complex combustion problems like turbulent flames simulated with DNS [20].

As CEMA is based on single-point thermo-chemistry information, it can be applied to the sample space ψ of the PDF formulation. From the n-th stochastic field stochastic field, an explosive mode λ_e^n can be obtained. The filtered explosive mode (function of space and time) is obtained by

$$\widetilde{\lambda}_e = \frac{1}{N} \sum_{n=1}^{N} \lambda_e^n \tag{18}$$

And a measure of the sub-grid fluctuations of the explosive mode, $\lambda_{e,sgs}$, is similarly obtained by applying (11) , viz.

$$\lambda_{e,sgs} = \sqrt{\left| \frac{1}{N} \sum_{n=1}^{N} (\lambda_e^n)^2 - (\widetilde{\lambda}_e)^2 \right|} \tag{19}$$

3.   Test Case

3.1   Experimental and Numerical Set-Up

The flame chosen in this study is the piloted, natural gas, non-premixed Delft III Flame. Despite its moderate Reynolds number, the Delft Flame has strong extinction and significant finite rate chemistry effects. It has only been investigated before by Merci et al. [22, 23] using RANS-PDF and by Ayache and Mastorakos [2] using a LES-CMC method.

The flame is composed of a central fuel jet, surrounded by two concentric co-flows of air. The central fuel jet has a bulk exit velocity of 21.9 m/s, corresponding to a Reynolds number Re = 9700 based on the jet diameter. The primary (inner) airflow velocity is 4.4 m/s and the secondary (outer) air flow velocity is 0.3 m/s. The fuel jet diameter is $D_{jet} = 6$ mm. The primary air annulus has an inner diameter of 15 mm and an outer diameter of 45 mm. The main fuel jet is separated from the primary air stream by a rim of outer diameter 15 mm. The pilot flames are located on this rim and consist of 0.5 mm diameter holes located on a circle of 7 mm diameter in order to prevent flame lift-off [22]. The fuel used was commercially available Dutch natural gas (see composition in Table 1) with an adiabatic temperature $T_{ad} = 2216$ K and a stoichiometric mixture fraction $f_{st} = 0.071$ [28].

The present work focuses on the area close to the nozzle exit and the solution domain therefore extends 27 jet diameters in the downstream direction and 8 diameters in the radial direction. The selected LES grid used is composed of $192 \times 88 \times 42$

Table 1. Fuel Composition (Mass Fractions)

Species	Jet
CH_4	70.13%
C_2H_2	0.0695%
C_2H_4	0.289%
C_2H_6	4.873%
C_3H_8	1.1155%
CO_2	2.1%
N_2	21.54%

cells in the longitudinal, radial and azimuthal direction respectively. Grid stretching in the radial directions was applied to resolve the gradients that arise near the inlet and in the shear layer of the flame and 20 grid points in the radial directions are located within the fuel jet stream. The minimum mesh size in radial direction occurs at the shear layer and flame position where $\Delta \approx 0.14$ mm, which is slightly finer compared to the most recent studies ($\Delta \approx 0.18$ mm according to [2]).

Free stream boundary conditions have been employed for all lateral boundaries and a convective outflow condition has been applied at the outflow plane [1] . Azimuthal perturbations were superimposed to the mean inflow profiles to mimic inflow turbulence [6]. The associated mean velocity fluctuations were taken from turbulent kinetic energy measurements at the inlet of the flow. The method has proven to be successful in reproducing turbulent characteristics of jet flames [27, 29].

In the experiment, the surrounding pilot flames are fed with a premixed acetylene/hydrogen/air mixture with an equivalence ratio ϕ of 1.4 and a C/H ratio equal to that of the natural gas [28]. The pilot mass flow rate ($\approx 2 \cdot 10^{-5}$ kg/s) and momentum ($\approx 2 \cdot 10^{-3}$ N) are small compared to the fuel's ($\approx 5 \cdot 10^{-4}$ kg/s and $2 \cdot 10^{-2}$ N) or air's ($\approx 8 \cdot 10^{-3}$ kg/s and $3 \cdot 10^{-2}$ N) inlet and therefore the flow is not going to be largely disturbed by it. Additionally, the pilot flame thermal power is small (approximately 1% of the total thermal power), therefore neglecting the pilot flames is a realistic approximation. Several approaches have been proposed in the literature with regards to the modelling of the pilot flames. Merci et al. [22, 23, 24], Roekaerts et al. [33] modelled the pilot flames by the local addition of a heat source term, neglecting their negligible mass flow rate and momentum. Ayache and Mastorakos [2] represented the pilot as an annular ring of 1 mm thickness around the fuel jet and this approach has been followed in the present work. The pilot composition was taken as the fully burnt stoichiometric mixture of the jet fuel and air, with the same mass flow rate as in the experiment. The inlet temperature was taken as 2087 K to match the temperature profiles in the first station.

To compute the chemical source term, a 19-species (H_2, H, O_2, OH, H_2O, HO_2, H_2O_2, CH_3, CH_4, CO, CO_2, CH_2O, C_2H_2, C_2H_4, C_2H_6, NH_3, NO, HCN and N_2), $15-$step augmented reduced mechanism (ARM) is used [37], derived from the complete GRI 3.0 skeletal mechanism using quasi-steady assumptions. The mechanism has been extensively validated and the laminar flame speed obtained with the chemical kinetics agrees very well with experimental data for the stoichiometric mixtures in this work.

In stiff ODE integrators, the Jacobian matrices are often evaluated through numerical perturbation of the variables and re-evaluation of the functions involved. This numerical approach is needed when the detailed mechanism is not available and analytical solutions are not possible. However, such perturbation approach may introduce errors in the evaluation of the smaller eigenvalues of the Jacobian. This is particularly important for CEMA because the chemical explosive modes are typically much slower than the fast modes due to the fast reacting radicals.

8

Therefore, analytic-derived Jacobian provides a better accuracy in calculating the Chemical Explosive Modes. To compare both approaches, analytic Jacobians from a CSP-reduced mechanism obtained from GRI3.0 [19] were also derived. It has to be noted that the similarity of the two chemical mechanisms (ARM and CSP) with only three minor species different, allowed to easily convert from the ARM field to CSP field. Afterwards, the simulation was continued with the CSP mechanism to phase out all the transients because of the chemistry change and therefore the CSP analytical jacobian analysis was performed on the species field based solely on the CSP chemistry mechanism.

4.   Results

The results section is structured as follows: First, the qualitatively behaviour of the flame is presented; where instantaneous and time-averaged results are shown. Then a qualitative picture of extinction will be introduced by investigating a sequence of filtered results and three-dimensional plots. A quantitative comparison with experimental measurements with and without model will be then presented and the effects of the turbulence-combustion model investigated. In a subsequent sub-section, the CEMA will be presented based on a snapshot of the species data.

4.1   Flow and Chemical Species

The qualitative behaviour of the flame can be observed in the instantaneous snapshots and time-averaged distributions in Figure 1. Between the fuel jet and the primary co-flow, the 3.5 mm rim creates a small recirculation zone, which provides an additional mechanism to stabilise the flame, in addition to the pilot stream. Figure $1-2a$ shows the instantaneous temperature distribution. The pockets of extinction are apparent throughout the flame, but especially close to the nozzle exit. The OH distribution is indicative of the instantaneous flame position [2]. The figure shows that the reaction zone is narrow compared to other piloted flames, such as Sandia Flame F, due to the absence of premixing in the fuel jet [2].

The reaction zone distribution is not strongly convoluted close to the burner. This can be attributed to the low stoichiometric mixture fraction which places the reaction zone in the lean side of the shear layer where the shear stresses are relatively low. As turbulence develops further downstream, the reaction zone is distorted significantly. The above mentioned observations are qualitatively consistent with the experiments and other numerical simulations [2]. Figure 2 shows sequential instantaneous plots of temperature and OH concentrations close to the nozzle exit when large extinction events are observed. A large extinction pocket (about 5 mm in size) is observed at 26 ms, the flame is then reconnected (indicated by the red circle in Fig. 2) after 4 ms. These extinction-reconnection events are happening continuously in the flame.

The size of the extinction pockets can be seen through the three-dimensional snapshots in Figure 3. The first plot shows the Stoichiometric iso-surface, coloured with temperature. The high range of temperatures on the surface is apparent. The extinction pockets are of the size of the jet diameter. Figure 3 (b) shows the instantaneous $T = 1500$ K iso-surface, coloured with OH mass fraction. The non-continuous flame surface is a clear indication of the large pockets of extinction; in particular in the 60 to 120 mm range.

Figures 4-6 show the radial profiles of the axial velocity, the temperature, the mixture fraction and the major reaction species at four axial positions downstream
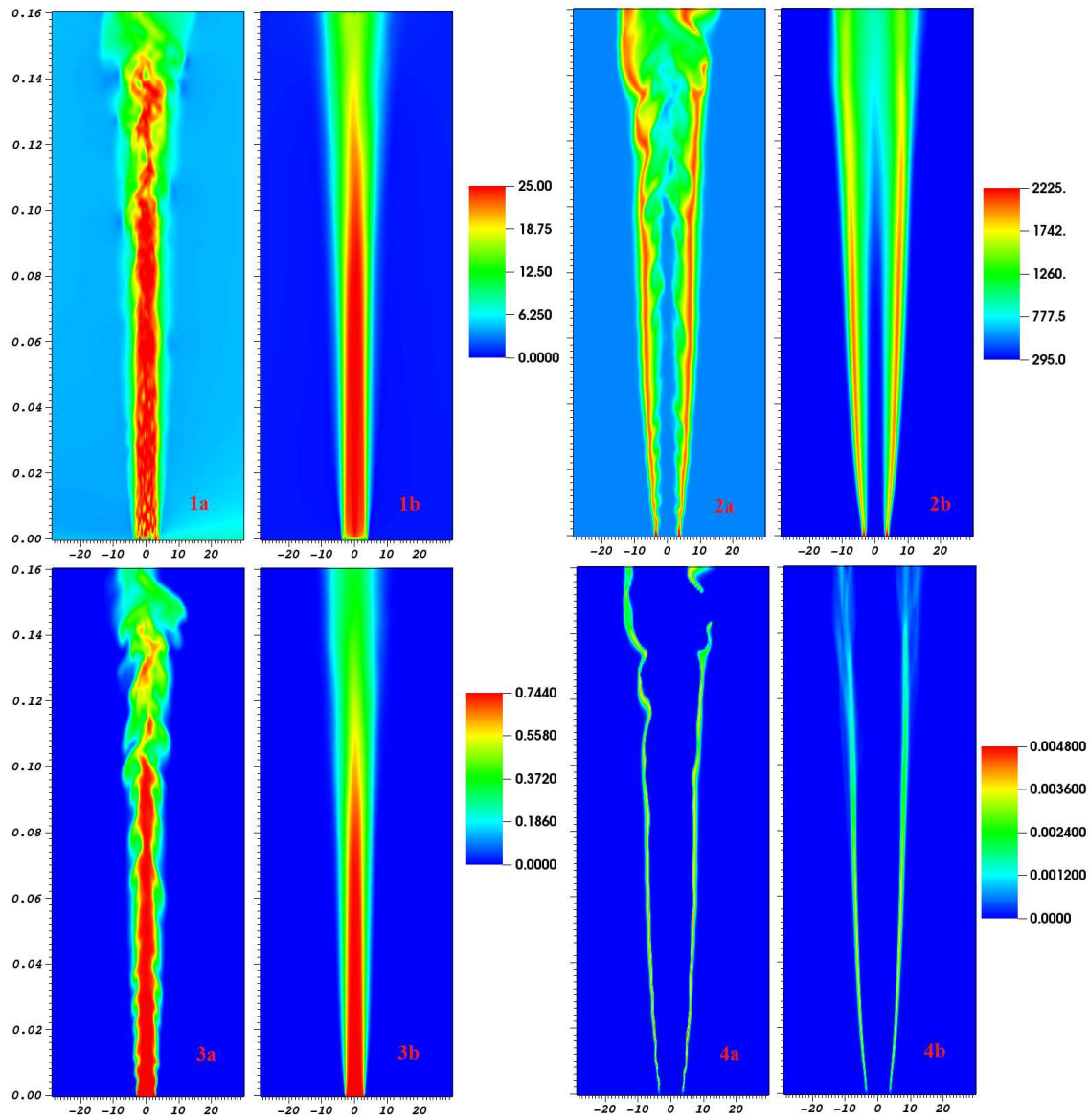
Figure 1.   Instantaneous and mean images of axial velocity (upper left), temperature (upper right), CH_4 (lower left) and OH mass fraction (lower right). Mean values are averaged over 10000 steps, corresponding to approximately 20 ms.

of the nozzle exit. The results show simulations with one stochastic field (no sub-grid modelling is performed) and $N = 8$ stochastic fields (following [26]). The inclusion of sub-grid effects improves the predictions, especially in the temperature close to the nozzle (the first axial station at 25 mm) is apparent. Improvements in the prediction of the mixture fraction and the CH_4 mass fraction close to the nozzle are also apparent. CO and OH is also much better predicted, indicating the accurate prediction of the location of the flame front. Finally, as it would be expected, NO is significantly over-predicted downstream the second axial station. This over-prediction has also been observed with GRI3.0-derived mechanism in similar flames [4].
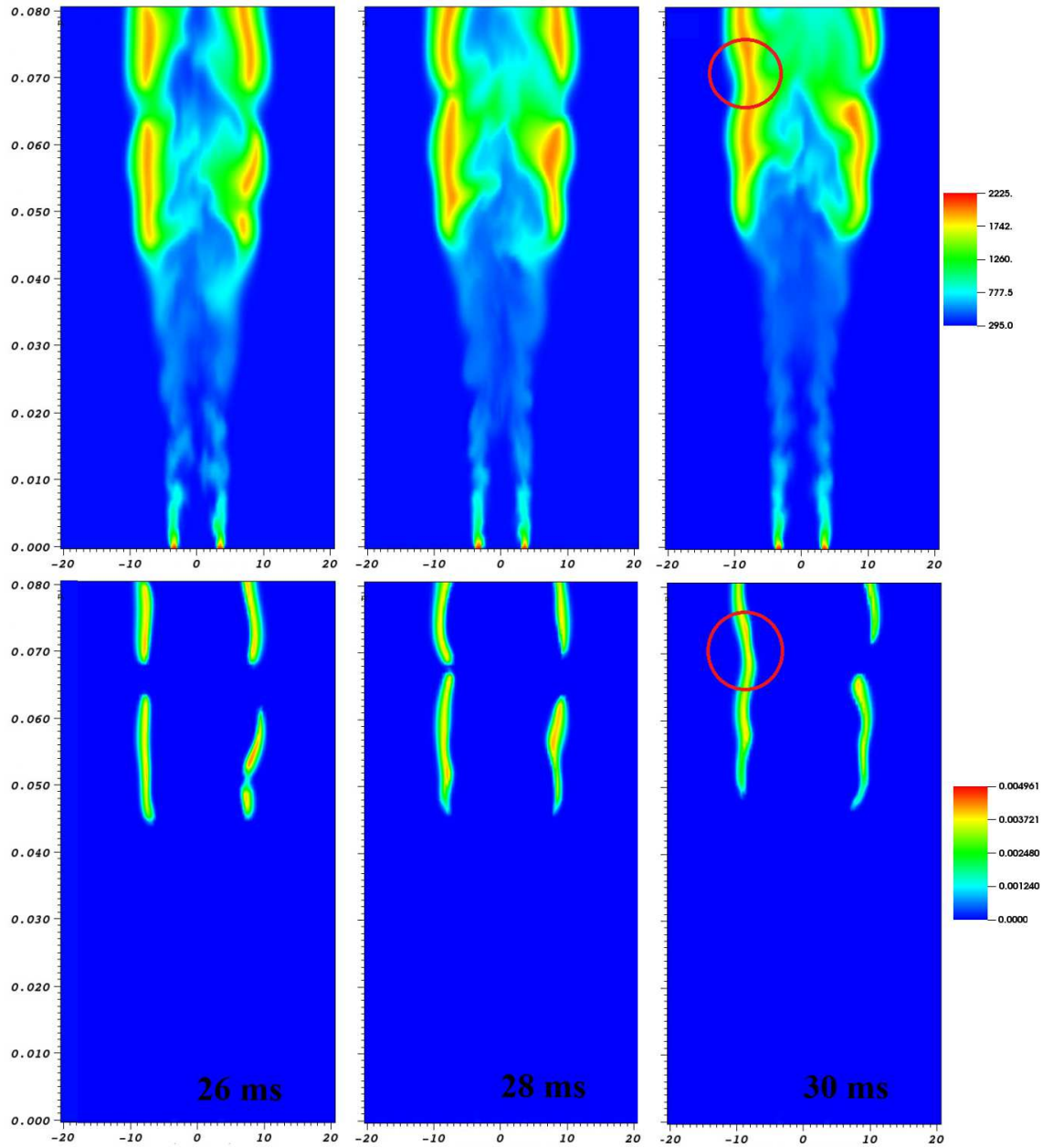
Figure 2. Three snapshots taken at 2 ms intervals of Temperature (upper row) and OH mass fraction (lower row). The reconnection event is indicated by the red circles.
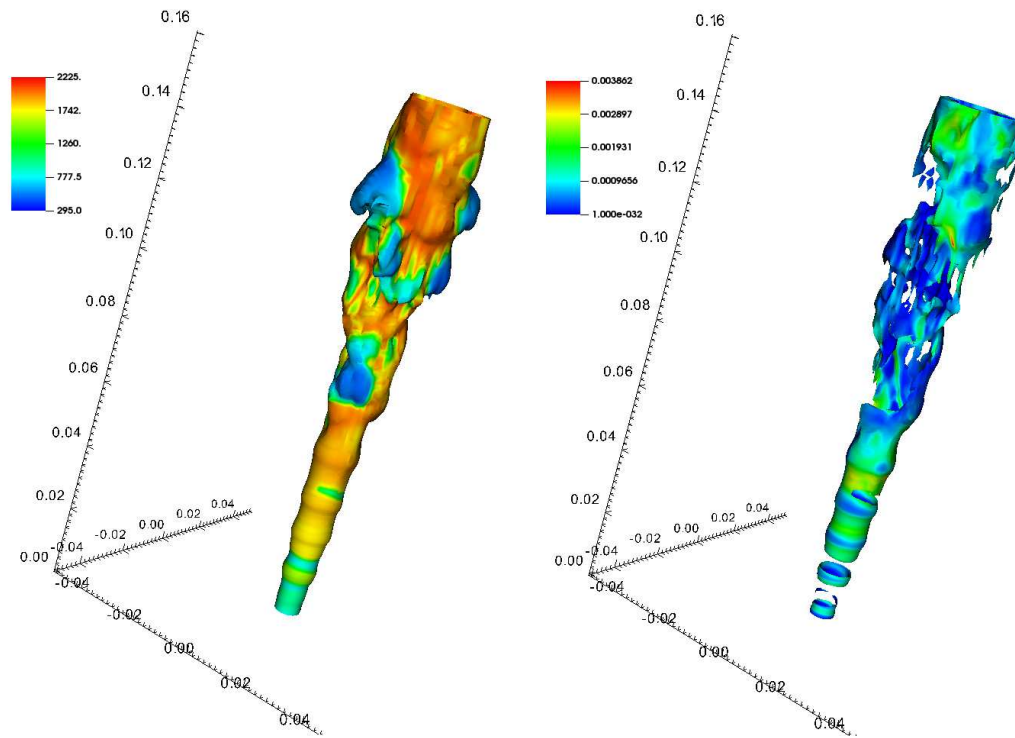
Figure 3. (a): Instantaneous snapshot of the flame front ($f_{st} = 0.0715$) coloured with temperature values. (b): Instantaneous snapshot of the $T = 1500$ K iso-surface, coloured with OH mass fraction contours.
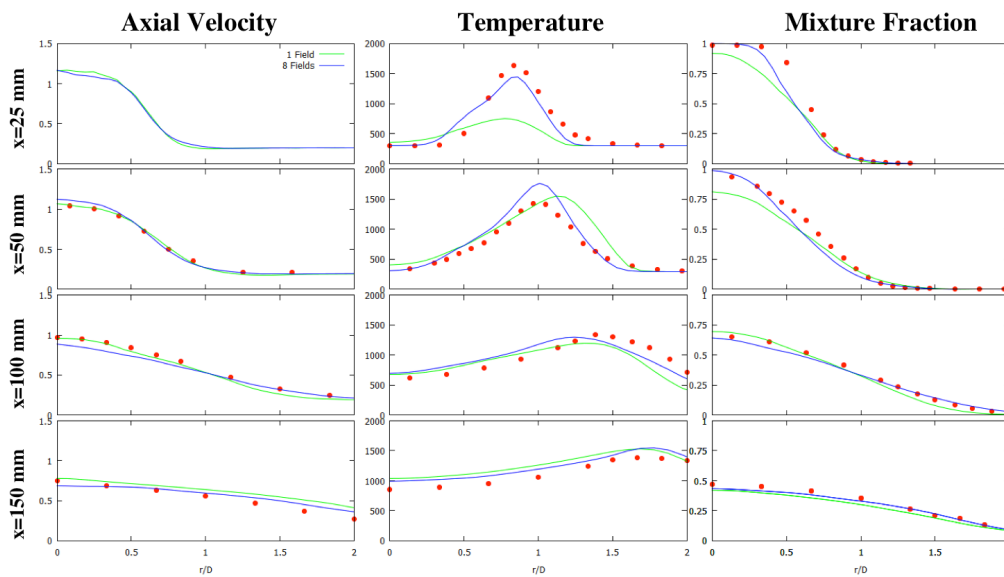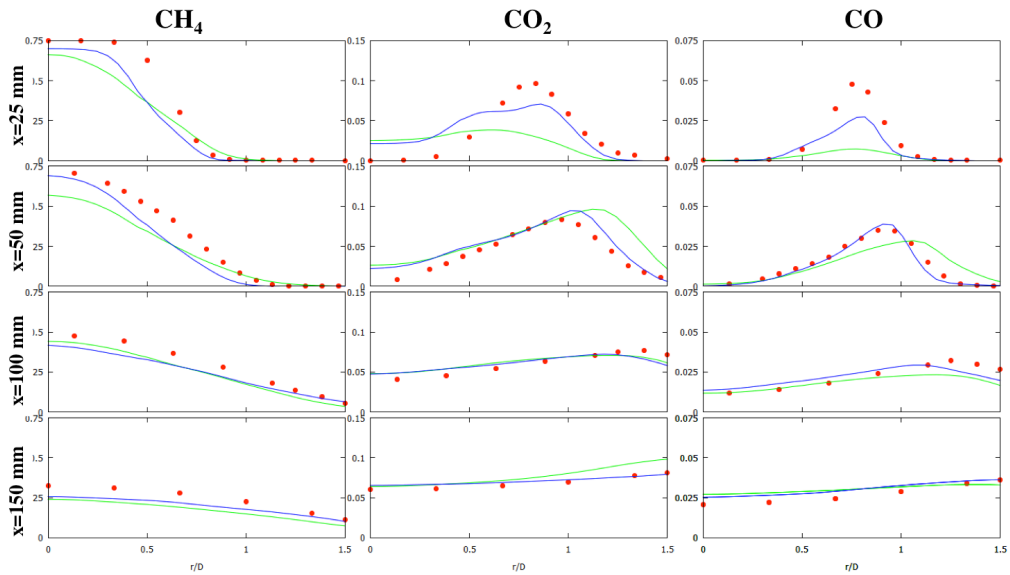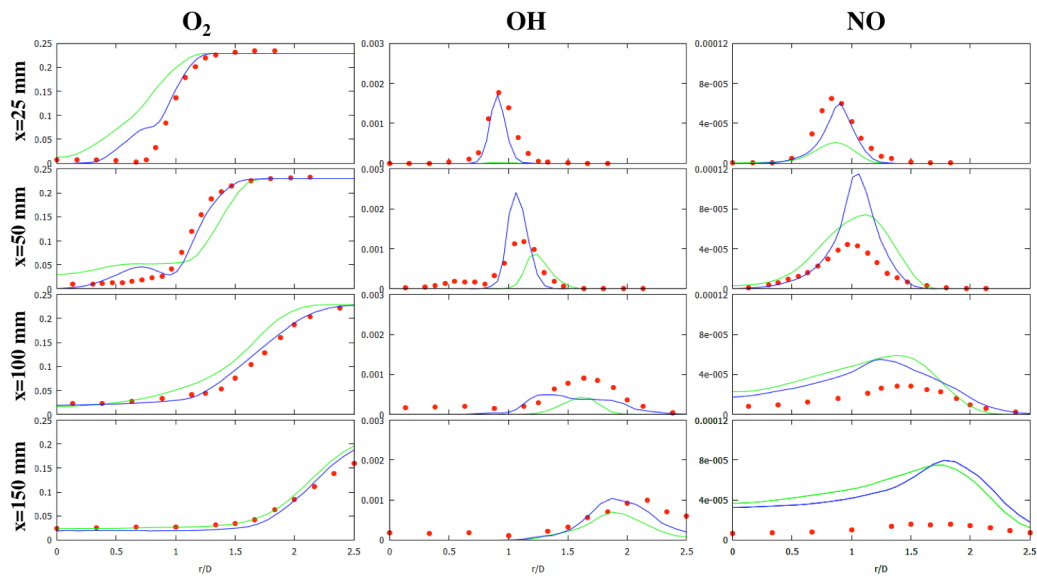

Figure 4. Mean axial velocity, temperature and mixture fraction radial distributions. The green line indicate results with $N = 1$ (no sub-grid model) and the blue results with $N = 8$. The symbols represent experimental data. Refer to the online colour version for the legend.

12

Figure 5. Mean CH_4, CO_2 and CO mass fraction radial distributions. Symbols as Fig. 4

Figure 6. Mean O_2, OH and NO mass fraction radial distributions. Symbols as Fig. 4

4.2   Chemical Explosive Mode Analysis

The Chemical Explosive Mode Analysis is applied to the Delft III flame at at approximately 28 ms after the start of the simulation, when the initial transients have been phased out.
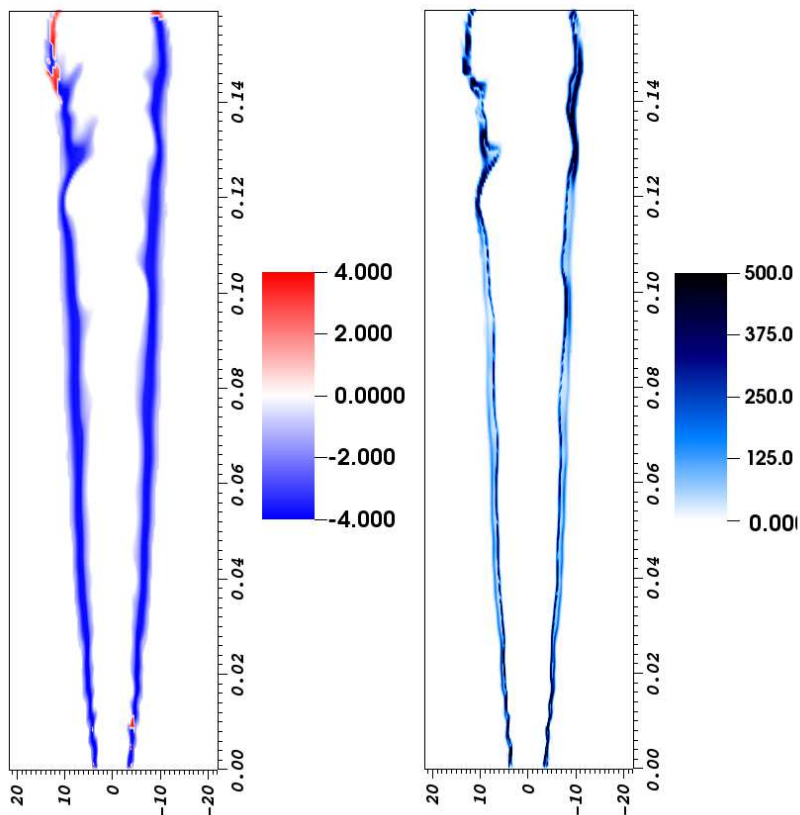

Figure 7. (a) Snapshot of $sign(\widetilde{\lambda_e}) \times \log\left[max(1, |\widetilde{\lambda_e}|)\right]$. (b) Snapshot of $\lambda_{e,sgs}$

Figure 7 shows the time scales of CEM. Pre-ignition mixtures with $\widetilde{\lambda_e} > 0$ are shown in red and post-ignition mixtures, $\widetilde{\lambda_e}$, in blue. Therefore, dark red denotes a highly explosive mixture and dark blue denotes near-equilibrium mixture; where all the eigenvalues λ_k are negative (and the explosive mode does not exist). Figure 7 (a) shows that in general, negative $\widetilde{\lambda_e}$ values are observed throughout the flame. The extinction regions are seen through regions of positive $\widetilde{\lambda_e}$ (shown in red), that are predominant close to the nozzle, although they are larger in size further downstream.

The explosive mode sub-grid fluctuations $\lambda_{e,sgs}$, are an indication of the different chemistry behaviour at sub-grid scales. A small value of $\lambda_{e,sgs}$ would indicate that the chemistry behaves very similar at the smallest scales. $\lambda_{e,sgs}$ acquires the highest values close to the nozzle, suggesting that sub-grid effects may be stronger there. Although there are definitely sub-grid fluctuations in the reaction zone, the intensity decreases downstream in the flame. The sub-grid scale effects seem to have a limited effect, in agreement with the temperature profiles shown in figure 4.

Figure 8 shows the CEM obtained by the evaluation the Jacobian using a numerical approximation and an analytical approach. In both cases, the same initial scalar field was used as a basis for the analysis. Due to the nature of the flame, no large qualitative discrepancies are observed between the two λ_e plots, suggesting

14

that the overall flame structure is captured correctly. However the numerical ja-
cobian method introduces high frequency noise that arises as spurious extinction
regions outside the flame front. Additionally, the magnitude of the ignition spots
may not be so accurately captured in the numerical Jacobian solution, as can be
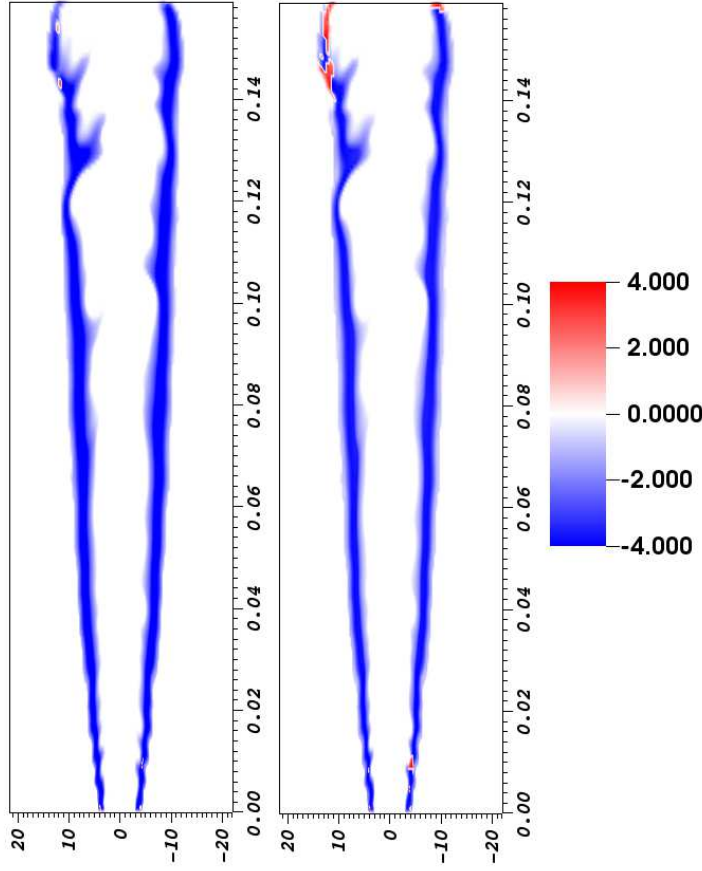seen by comparing the red spots in both subplots of the same figure.

Figure 8.   Snapshot of $sign(\widetilde{\lambda_e}) \times \log\left[max(1, |\widetilde{\lambda_e}|)\right]$. Results obtained with Numerical Jacobians (a) and
Analytical (b). Contours as Fig. 7(a)

Turbulence-Chemistry interaction is characterised by the Damköhler number,
which relates chemical and flow time-scales. The chemical time-scale relevant to
extinction in CEMA is λ_e. For the n-th stochastic field, a Damköhler number can
be defined as [20, 21, 40]:

$$\mathrm{Da}^n = \lambda_e^n \cdot \chi^{-1} = \frac{\lambda_e^n}{2D|\nabla f^n|^2} \tag{20}$$

In a similar way to the sub-grid CEM (19), a sub-grid Damköhler number is
defined as

$$\mathrm{Da}_{sgs} = \sqrt{\left|\frac{1}{N}\sum_{n=1}^{N}(\mathrm{Da}^n)^2 - (\widetilde{\mathrm{Da}})^2\right|} \tag{21}$$

Where the filtered Damköhler number, $\widetilde{\mathrm{Da}}$, is obtained form the filtered explosive
mode and filtered scalar dissipation. $\widetilde{\mathrm{Da}} \sim 1$, indicates that flow and time scales are

comparable and large scale (greater than filter size) extinction occurs. Due to the low number of statistical samples and the shapes of the sub-grid PDFs, Da_{sgs} may not be sufficient to fully characterised sub-grid extinction. However, $Da_{sgs} \sim \widetilde{Da}$ would suggest that sub-grid extinction *may* be present.
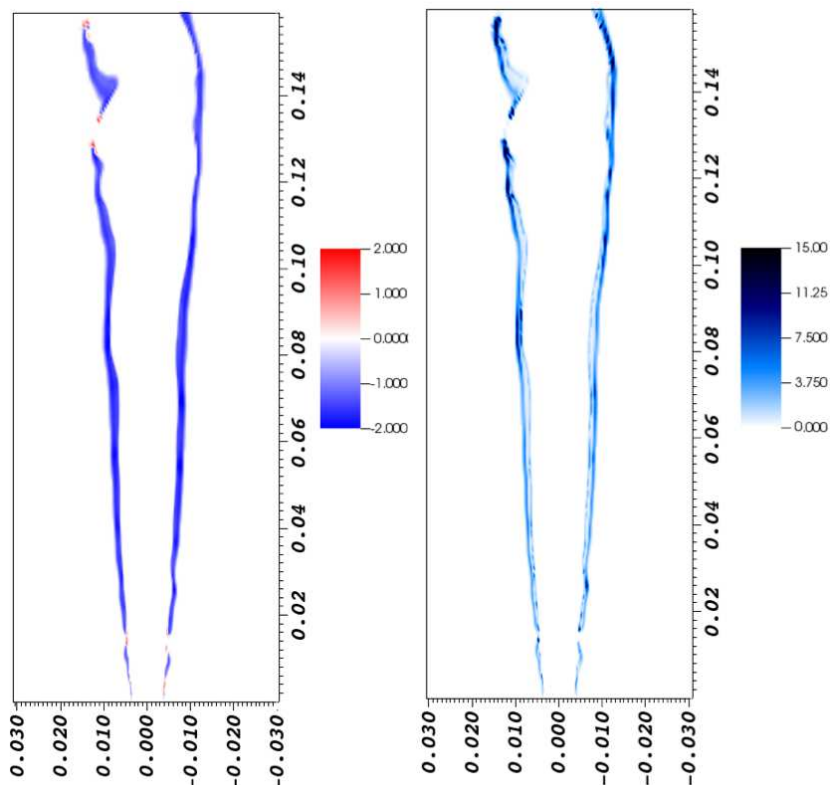

Figure 9. (a) Snapshot of $sign(\widetilde{\lambda_e}) \times \log\left[max(1, |\widetilde{Da}|)\right]$. (b) Snapshot of Da_{sgs}

In Figure 9, $\widetilde{Da}$ and Da_{sgs} are shown. Extinction observed in Figure 2 is characterized by low $\widetilde{Da}$, see Figure 9(a). The comparison of the absolute maximum Damköler values ~ 300) and the sub-grid scale $Da_{sgs} \sim 10 - 25$ (see Figure 9(b)), suggest Damköler fluctuations are of the order of 10%, and extinction cannot be attributed to sub-grid scale effects. Figure 10 shows that the ratio $Da_{sgs}/\widetilde{Da}$ is small everywhere $(10 - 20\%)$ and only close to the nozzle $Da_{sgs} \sim \widetilde{Da}$. In general, extinction observed in this flame is on the large (super-grid) scale and sub-grid scale effects do not contribute to extinction, except close to the nozzle. Additional sub-grid modelling effort will not be beneficial.

The area close to the nozzle exit shows low Damköler numbers close to unity and the sub-grid scale Da_{sgs} is relatively low. In the same region, there can be observed positive λ_e in figure 7, indicating that at this region the flame is supported by auto-ignition, but only on a local and instantaneous basis. In order to emphasise on this feature, another instantaneous extinction pocket is selected, approximately 12 mm downstream of the nozzle exit and the results shown in figure 11. In this figure, two consecutive extinction pockets are observed, both of them far away from the nozzle exit. Both of them have large Da_{sgs} fluctuation at the tips of the extinction pockets and positive $\widetilde{\lambda_e}$ values inside the extinction pockets. This supports the above observation, indicating that throughout the flame (and not only limited in the nozzle exit region), whenever localised extinction appears, re-ignition is the mechanism that instantaneously and locally supports the flame and prevents it
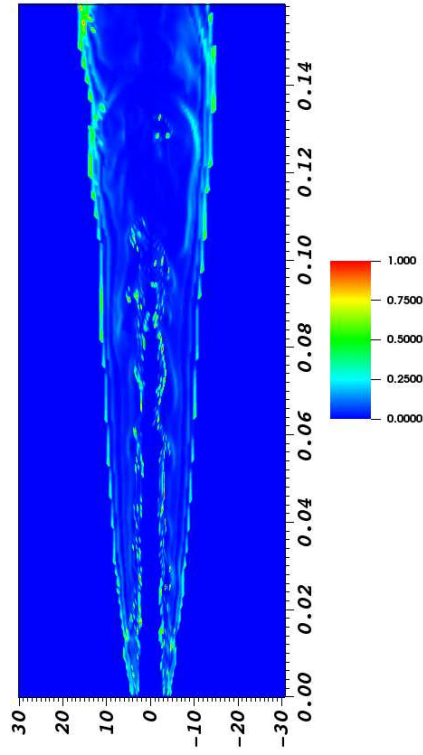
Figure 10. Snapshot of the $\mathrm{Da}_{sgs}/\widetilde{\mathrm{Da}}$ ratio.
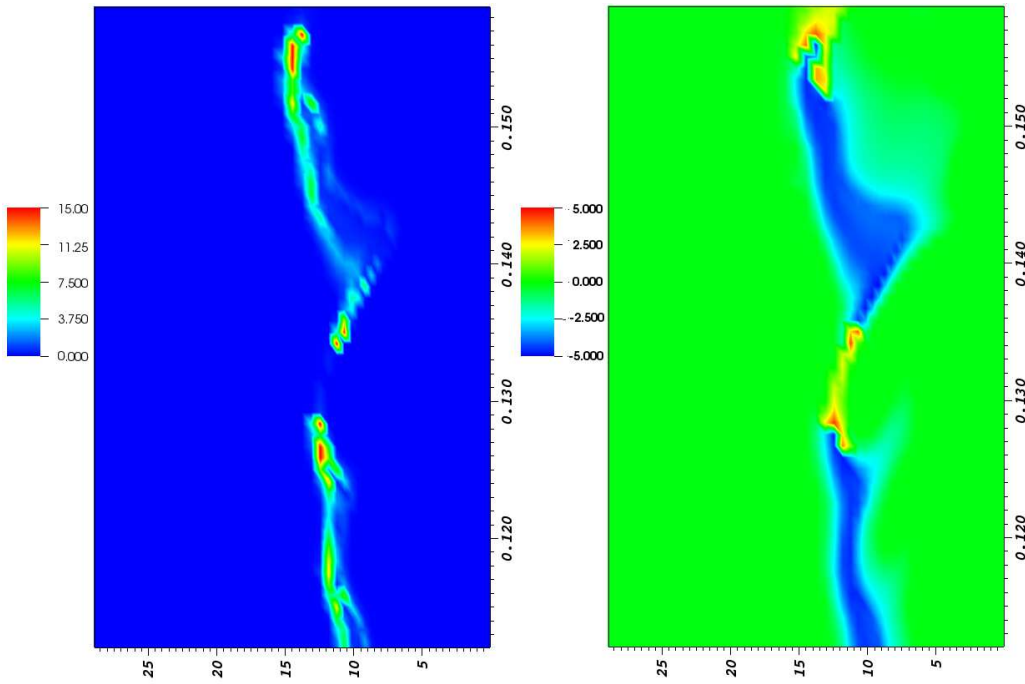
from quenching.

Figure 11.   Detailed CEMA view of an extinction pocket, 12 mm downstream of the nozzle exit, at 28.4 ms (a) Da_{sgs} (b) $sign(\widetilde{\lambda_e}) \times \log\left[max(1, |\widetilde{\lambda_e}|)\right]$

To further determine the structure of the Delft III flame, Figures 12 and 13 show the explosion and participation index; identified with **EI** given from equation (16) and **PI** given from equation (17).
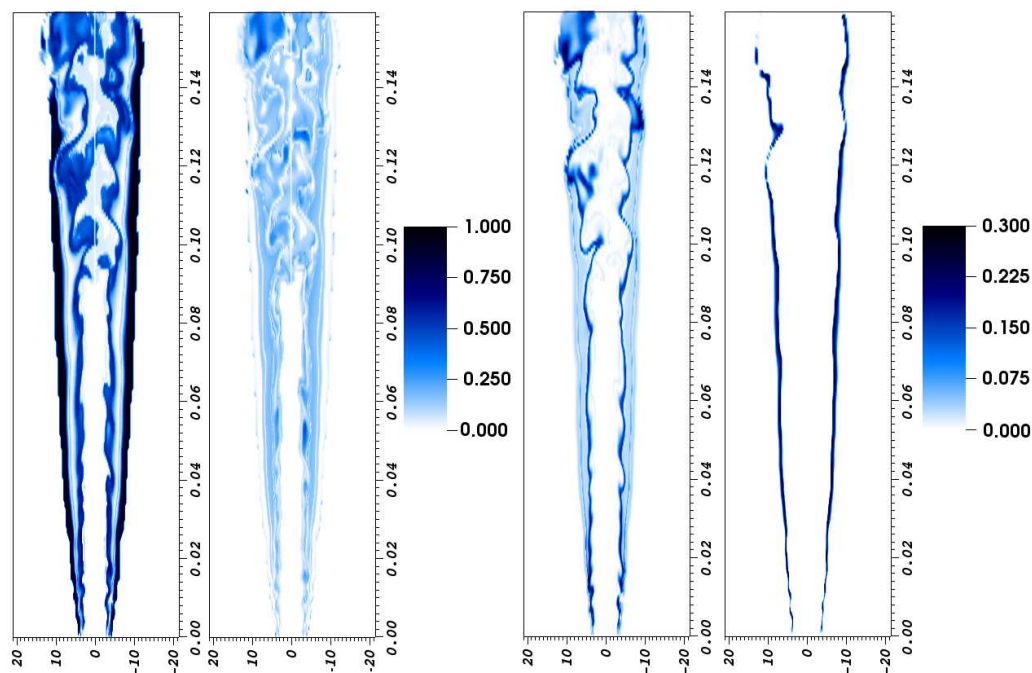
Figure 12.   Explosion Index (EI) plots of the four species with the largest average contribution to CEM
From left to right: C_2H_2, H_2, C_2H_4 and H.

The explosion index analysis (Figure 12) indicates that the species with largest average contribution to CEM are C_2H_2, H_2, C_2H_4 and H. The explosive index of C_2H_2 and H acquire large values at the reaction zone. The associated index of hydrogen and ethylene are largest in the inner part of the flame; where CEM is smallest (see Fig. 7)

The Participation Index (PI) analysis indicates that the reactions with largest contributions to the CEM are the following reactions in the skeletal mechanism

- Reaction No. 33: $H + O_2 + H_2O \leftrightarrow HO_2 + H_2O$
- Reaction No. 35: $H + O_2 \leftrightarrow O + OH$
- Reaction No. 40: $H + OH + M \leftrightarrow H_2O + M$
- Reaction No. 49: $H + CH_3 \leftrightarrow CH_4$
- Reaction No. 94: $OH + CO \leftrightarrow H + CO_2$
- Reaction No. 111: $HO_2 + CH_3 \leftrightarrow OH + CH_3O$

The contributions of each reaction the CEM depends locally on the flame structure. In the flame region, the exothermic oxidation of CO to CO_2 is the dominating mechanism. The extinction pocket observed in Figure 9 corresponds to low **PI** of reactions No. 33, 40 and 94. These reactions control the re-ignition mechanism that prevent the flame from quenching. Close to the nozzle, flame extinction cannot be attributed to these reactions and is probably more related to other reactions with lower global **PI**.
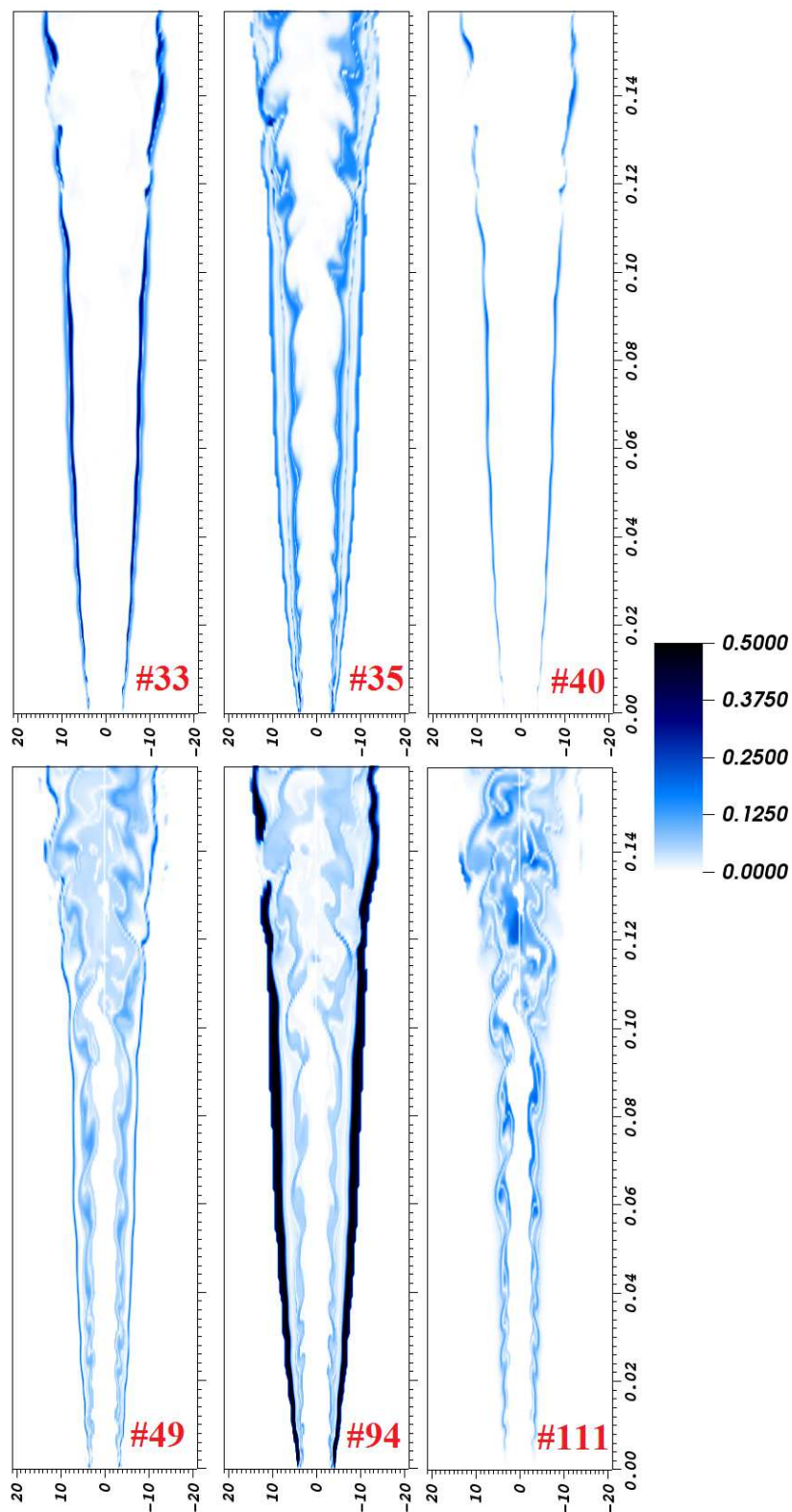
18

Figure 13. Participation Index (PI) plots of the four reactions with the largest average contribution to CEM (Reaction No. 33, 35, 40, 49, 94 and 111).

5.   Conclusions

The present paper analyses extinction of a non-premixed flame using a LES-PDF approach combined with a-posteriori explosive mode analysis. The studied test case, the Delft III flame, shows quenching with large extinction pockets despite the moderately low Reynolds number. The major flame characteristics (flow field, temperature and species concentrations) were accurately captured by the simulation. The introduction of stochastic fields, to account for sub-grid fluctuations, improves the predictions close to the nozzle exit, however its effects are minor further downstream. This relatively low importance of the sub-grid model can be attributed to the relatively low Reynolds Number of the flame.

The Chemical Explosive Mode Analysis was successfully applied to the studied flame. The CEM analysis clearly identifies the regions with extinction, which are marked by a positive explosive mode. The distribution of Da_{sgs} suggest that sub-grid effects in the studied flame do not contribute to extinction. Two type of extinction pockets are detected: close to the nozzle exit, where quenching regions are relatively uniform and sub-grid fluctuations may have a contribution, and downstream where large extinction regions are observed ($\sim D_{jet}$) and sub-grid effects are not that important. In both regions mean Da is close to unity. Sub-grid Damköhler fluctuations are largest at the edge of the extinction pocket. The explosive mode,λ_e, is positive in the extinction pocket, which indicates that re-ignition is the stabilisation mechanism and not flame propagation from neighbouring triple flames. This is supported by the Explosion Index and Participation Index analysis; where species such as C_2H_2, H_2, C_2H_4 and H have uninterrupted **EI** through the flame.

The paper has shown the potential of the combined LES-PDF method and CEMA to understand flame structure and extinction in turbulent flames. Due to the underlying synergies of CEMA and the stochastic fields approach, the process can be applied directly to high Reynolds number flames as well as complex configurations.

References

[1] K. Akselvoll and P. Moin. Large Eddy Simulation of Turbulent Confined Coannular Jets. *J. Fluid Mech.*, 315:387–411, 1996.

[2] S. Ayache and E. Mastorakos. Conditional Moment Closure/Large Eddy Simulation of the Delft-III Natural Gas Non-premixed Jet Flame. *Flow Turb. Combust.*, 88(1-2):207–231, 2012.

[3] N. Branley and W. P. Jones. Large Eddy Simulation of a Turbulent Non-premixed Flame. *Combust. Flame*, 127(1):1914–1934, 2001.

[4] R R Cao and S B Pope. The influence of chemical mechanisms on PDF calculations of nonpremixed piloted jet flames. *Combust. Flame*, 143(4):450–470, December 2005.

[5] R R Cao, H Wang, and S B Pope. The effect of mixing models in PDF calculations of piloted jet flames. *Proc. Combust. Inst.*, 31(1):1543–1550, January 2007.

[6] I. Danaila and B. Jan Boersma. Direct Numerical Simulation of Bifurcating Jets. *Phys. Fluids*, 12 (1255):387–411, 2000.

[7] F. Di Mare. *Large Eddy Simulation of Reacting and non-Reacting Turbulent Flows*. PhD thesis, Imperial College, 2002.

[8] I. A. Dodoulas and S. Navarro-Martinez. Large Eddy Simulation of Premixed Turbulent Flames Using the Probability Density Function Approach. *Flow Turb. Combust.*, 90(3):645–678, 2013.

[9] C. Dopazo and E. O' Brien. Functional Formulation of non-Isothermal Turbulent Reactive Flows. *Phys. Fluids*, 17(11), 1974.

[10] F Gao and E E O'Brien. A large-eddy simulation scheme for turbulent reacting flows. *Phys. Fluids*, 5(6):1282–1284, 1993.

[11] A. Garmory and E. Mastorakos. Capturing Localised Extinction in Sandia Flame F with LES−CMC. *Proceedings of the Combustion Institute*, 33(1):1673–1680, 2011.

[12] D. A. Goussis and S. H. Lam. A Study of Homogeneous Methanol Oxidation Kinetics Using CSP. *Proc. Combust. Inst.*, 24(1):113–120, 1992.

[13] W. P. Jones and S. Navarro-Martinez. Large Eddy Simulation of Autoignition with a Subgrid Probability Density Function Method. *Combust. Flame*, 150(3):170–187, 2007.

[14] W. P. Jones and S. Navarro-Martinez. Large Eddy Simulation and the Filtered Probability Density Function Method. *AIP Conference Proceedings*, pages 39–62, 2009.

[15] W. P. Jones and V. N. Prasad. Large Eddy Simulation of the Sandia Flame Series (D-F) using the Eulerian Stochastic Field Method. *Combust. Flame*, 157(9):1621–1636, 2010.

[16] W. P. Jones, A. J. Marquis, and V. N. Prasad. LES of a Turbulent Premixed Swirl Burner Using the Eulerian Stochastic Field Method. *Combust. Flame*, 159(10):3079–3095, 2012.

[17] W.P. Jones, F. di Mare, and A.J. Marquis. BOFFIN-LES : User's Guide. 2002.

[18] W. Liu, A. P. Kelley, and C. K. Law. Flame Propagation and Counterflow Non-Premixed Ignition of Mixtures of Methane and Ethylene. *Combust. Flame*, 157(5):1027–1036, 2010.

[19] T Lu and C K Law. A criterion based on computational singular perturbation for the identification of quasi steady state species: A reduced mechanism for methane oxidation with {NO} chemistry. *Combust. Flame*, 154(4):761 – 774, 2008. ISSN 0010-2180.

[20] T. F. Lu, C. S. Yoo, J. H. Chen, and C. K. Law. Three-dimensional Direct Numerical Simulation of a Turbulent Lifted Hydrogen Jet Flame in Heated Coflow: A Chemical Explosive Mode Analysis. *J. Fluid Mech.*, 652:45–64, 2010.

[21] Z. Y. Luo, C. S. Yoo, E. S. Richardson, J. H. Chen, C. K. Law, and T. F. Lu. Chemical Explosive Mode Analysis for a Turbulent Lifted Ethylene Jet Flame in Highly-Heated Coflow. *Combust. Flame*, 159(1):265–274, 2012.

[22] B. Merci, B. Naud, and D. Roekaerts. Flow and Mixing Fields for Transported Scalar PDF Simulations of a Piloted Jet Diffusion Flame ('Delft Flame III'). *Flow Turb. Combust.*, 74(3):239–272, 2005.

[23] B. Merci, D. Roekaerts, and B. Naud. Study of the Performance of Three Micromixing Models in Transported Scalar PDF Simulations of a Piloted Jet Diffusion Flame (Delft Flame III). *Combust. Flame*, 144(3):476–493, 2006.

[24] B. Merci, B. Naud, and D. Roekaerts. Interaction Between Chemistry and Micro Mixing Modeling in Transported PDF Simulations of Turbulent Non Premixed Flames. *Combust. Sci. Technol.*, 179 (1-2):153–172, 2007.

[25] Y Mizobuchi, S Tachibana, J Shinio, S Ogawa, and T Takeno. A numerical analysis of the structure of a turbulent hydrogen jet lifted flame. *Proc. Combust. Inst.*, 29:2009–2015, 2002.

[26] R. Mustata, L. Valiño, C. Jimenez, W. P. Jones, and S. Bondi. A Probability Density Function Eulerian Monte Carlo Field Method for Large Eddy Simulations: Application to a Turbulent Piloted Methane/Air Diffusion Flame (Sandia D). *Combust. Flame*, 145(1-2):88–104, 2006.

[27] S. Navarro-Martinez, A. Kronenburg, and F. di Mare. Conditional Moment Closure for Large Eddy Simulations. *Flow Turb. Combust.*, 75:245–274, 2005.

[28] P. A. Nooren, M. Versluis, T. H. van der Meer, R. S. Barlow, and J. H. Frank. Raman-Rayleigh-LIF Measurements of Temperature and Species Concentrations in the Delft Piloted Turbulent Jet Diffusion Flame. *Applied Physics B-Lasers and Optics*, 71(1):95–111, 2000.

[29] H. Pitsch and H. Steiner. Large-Eddy Simulation of a Turbulent Piloted Methane/Air Diffusion Flame (Sandia Flame D). *Phys. Fluids*, 12(10):2541–2554, 2000.

[30] S B Pope. PDF Methods for Turbulent Reactive Flows. *Prog. Energy Combust. Sci.*, 11:119–192, 1985.

[31] V N Prasad, A R Masri, S Navarro-Martinez, and K H Luo. Investigation of auto-ignition in turbulent methanol spray flames using Large Eddy Simulation. *Combust. Flame*, 160(12):2941–2954, 2013.

[32] M H Protter and Weinberger H F. *Maximum Principles in Differential Equations.* Springer, 1999.

[33] D. Roekaerts, B. Merci, and B. Naud. Comparison of Transported Scalar PDF and Velocity Scalar PDF Approaches to 'Delft flame III'. *Comptes Rendus Mecanique*, 334(8-9):507–516, 2006.

[34] C. Schneider, A. Dreizler, J. Janicka, and E. P. Hassel. Flow Field Measurements of Stable and Locally Extinguishing Hydrocarbon Fuelled Jet Flames. *Combust. Flame*, 135(1-2):185–190, 2003.

[35] R. Q. Shan, C. S. Yoo, J. H. Chen, and T. F. Lu. Computational Diagnostics for n-heptane Flames with Chemical Explosive Mode Analysis. *Combust. Flame*, 159(10):3119–3127, 2012.

[36] J Smagorinsky. General circulation experiments with the primitive equations: I. The basic experiment. *Monthly weather review*, 91(3), 1963.

[37] C. J. Sung, C. K. Law, and J. Y. Chen. Augmented Reduced Mechanisms for NO Emission in Methane Oxidation. *Combust. Flame*, 125(1):906–919, 2001.

[38] Luis Valiño. A Field Monte Carlo Formulation for Calculating the Probability Density Function of a Single Scalar in a Turbulent Flow. *Flow Turb. Combust.*, 60(2):157–172, 1998.

[39] C. S. Yoo, T. F. Lu, J. H. Chen, and C. K. Law. Direct Numerical Simulations of Ignition of a Lean n-heptane/air Mixture with Temperature Inhomogeneities at Constant Volume: Parametric Study. *Combust. Flame*, 158(9):1727–1741, 2011.

[40] C. S. Yoo, E. S. Richardson, R. Sankaran, and J. H. Chen. A DNS Study on the Stabilization Mechanism of a Turbulent Lifted Ethylene Jet Flame in Highly-Heated Coflow. *Proc. Combust. Inst.*, 33:1619–1627, 2011.